International Journal of Solids and Structures 50 (2013) 4030–4042

Contents lists available at ScienceDirect

International Journal of Solids and Structures

journal homepage: www.elsevier.com/locate/ijsolstr

Frictional moving contact over the surface between a rigid punch and piezomagnetic materials – Terfenol-D as example

Yue-Ting Zhou, Tae-Won Kim *

School of Mechanical Engineering, Hanyang University, Seoul 133-791, Republic of Korea

ARTICLE INFO

Article history:
Received 12 March 2013
Received in revised form 22 July 2013
Available online 21 August 2013

Keywords:
Frictional moving contact
Piezomagnetic materials
Friction coefficient
Exact solutions
Surface damage

ABSTRACT

A general theory of the frictional moving contact of piezomagnetic materials indented by a flat or cylindrical punch is set up. The rigid punch moves at a constant speed and the Coulomb friction law applies inside the contact region. Terfenol-D with high magnetostriction and coupling is chosen. Employing the Galilean transformation and Fourier transform, Cauchy integral equations of the second kind are obtained and solved exactly. Closed-form expressions of physical quantities on the surface in terms of elementary functions are given. Numerical analyses are conducted to reveal the effects of the friction coefficient and moving speed of the punch on various surface stresses and magnetic induction. The singularity, discontinuity and spike of the surface magnetic induction may be important factors to explain why surface damage occurs for piezomagnetic materials.

1. Introduction

Among various branches of the emerging technologies of modern intelligent materials, piezomagnetic materials are an important one (Wu and Huang, 2000). Various applications of piezomagnetic materials, such as the development of magnetic storage and read-out devices, ultrasonic generators, magneto-mechanical transducers, magnetic sensors and stress sensors (Affane et al., 1996; Pinkerton et al., 1997; Shim et al., 1998; Karl et al., 2000), are found in industry practicing due to their magnetoelastic coupling effects between mechanical strain and the state of magnetization.

The magnetoelastic coupling effect of piezomagnetic materials has been measured by many researchers. Herbst et al. (1997) developed an approximate model to analyze the magneto-mechanical interaction for composites consisting of magnetostrictive particles dispersed in a nonmagnetostrictive matrix. Chen et al. (2003) demonstrated that there exists an exact connection between the effective magnetostriction and influence functions for the composite system by using an idea of Levin (1967), which was originally devised for the estimate of effective thermal expansion of composite materials. Extending the double-inclusion model to deal with magnetoelastic problems, Feng et al. (2003) made an attempt to predict the effective properties of magnetostrictive composites consisting of magnetostrictive particles dispersed in a nonmagnetostrictive matrix. Among various kinds of piezomagnetic materials, Terfenol-D ($Tb_{0.3}Dy_{0.7}FeO_{1.93}$) is a highly magnetostrictive alloy of iron and the rare-earth elements, terbium and dysprosium (Moffet et al., 1991), whose magnetoelastic coupling effect has also drawn attention. Chen et al. (1999) measured the dependence of saturated magnetostriction for Terfenol-D composites based on a model theory for the magnetostriction of such composites with two limiting assumptions: uniform strain or uniform stress inside the composite, and they concluded that to obtain a high magnetostriction and adequate mechanical properties of a composite, the elastic moduli of the magnetostrictive phase and the matrix should be as close as possible in value. Using a cold and hot compression-molding technique, Guo et al. (2001) produced the epoxy and glass matrix Terfenol-D composites and investigated the static and dynamic magnetic and magnetomechanical properties of samples as functions of bias field, frequency and ac drive field. Recently, Lukashev et al. (2008) showed that the magnetic structure of antiperovskite, such as Mn3GaN, can be controlled by a small applied biaxial strain and an appreciable net magnetization may appear in the strained system. More recently, Singh and Rokne (2013) studied the propagation of SH waves in two bonded semi-infinite material, one piezoelectric and the other piezomagnetic, in which the material properties of the two materials, including magneto-mechanical properties, vary in two directions, one parallel to the interface and the other perpendicular to the interface. Chen et al. (2013) developed a piezomagnetic force microscopy (PmFM) technique to enable quantitative probing of magnetic materials and structures at the nanoscale with high sensitivity and spatial resolution.

* Corresponding author. Tel.: +82 2 2220 0421; fax: +82 2 2292 0401.
E-mail addresses: zhouyt@hanyang.ac.kr (Y.-T. Zhou), twkim@hanyang.ac.kr (T.-W. Kim).

0020-7683/$ - see front matter © 2013 Elsevier Ltd. All rights reserved.
http://dx.doi.org/10.1016/j.ijsolstr.2013.08.015

Indentation technique is a simple method to measure the strength of the magnetization of piezomagnetic materials, which needs the solution of the corresponding contact problem. Giannakopoulos and Parmaklis (2007) proposed a general theory for the axisymmetric indentation of piezomagnetic solids subjected a flat rigid punch in a static state, and conducted an experiment on the material Terfenol-D. Zhou and Lee (2012) studied the moving contact behavior of piezomagnetic materials under the action of a frictionless sliding rigid punch. These two papers are about exact solutions of frictionless contact. For frictional contact, solutions of the flat punch (Guler and Erdogan, 2004) and cylindrical punch (Guler and Erdogan, 2007) acting on an elastic half-plane were given. Exact contact analysis for piezoelectric materials indented by a frictional sliding punch, which occupies a triangular or cylindrical profile, was conducted by Zhou and Lee (2013). In Guler and Erdogan (2004, 2007) and Zhou and Lee (2013), the frictional punch was stationary. To the authors' knowledge, the solution, not to mention exact solution, of frictional moving contact of piezomagnetic materials indented by a frictional flat or cylindrical punch has not been reported in the open literatures.

The present article sets up a model for the frictional moving contact of piezomagnetic materials under a rigid punch. The rigid punch possessing a flat or cylindrical profile moves at a constant speed. Coulomb friction law applies inside the contact region. The Galilean transformation is introduced to make the stated problem mathematically tractable. Based on the appropriate fundamental solutions, Cauchy type singular integral equations of the second kind are obtained and solved exactly. Explicit expressions of stress components and magnetic induction on the surface in terms of elementary functions are given. Numerical results for Terfenol-D are presented to show the influences of the friction coefficient and the moving velocity on the contact behavior. The surface damage mechanism is revealed.

2. Problem statement and formulation

2.1. Geometry and loading condition

A punch with a flat or a cylindrical foundation is acting on piezomagnetic materials placed in the coordinated system (x_1, x_3). The punch moves to the left at a constant speed V. Inside the contact region, friction law is of the Coulomb type, i.e.

$$Q = \mu_f \cdot P, \tag{1}$$

where P and Q, respectively, represent the resultant normal and tangential forces acting on the punch and μ_f is the friction coefficient.

2.2. Material properties

It has been shown that Terfenol-D is an important magnetostrictive material due to its high magnetostriction and coupling. Therefore, in this study, Terfenol-D is selected among piezomagnetic materials. The mechanical, piezomagnetic coefficients and permeability coefficients are taken as (Giannakopoulos and Parmaklis, 2007)

$$\begin{aligned} &c_{11} = 5.5\times10^{10}\ \mathrm{N/m^2}, \quad c_{13} = 4.3\times10^{10}\ \mathrm{N/m^2},\\ &c_{33} = 5.5\times10^{10}\ \mathrm{N/m^2}, \quad c_{44} = 1.2\times10^{10}\ \mathrm{N/m^2},\\ &qd_{15} = 0\frac{N}{Am}, \quad d_{31} = -45\frac{N}{Am}, \quad d_{33} = 90\frac{N}{Am},\\ &\mu_{11} = \mu_{33} = 6.23\times10^{-6}\frac{N^2}{A}, \end{aligned} \tag{2}$$

where c_{mn}, d_{mn} and μ_{mm} are elastic coefficients, piezomagnetic coefficients and permeability coefficients, respectively.

3. Basic equations and boundary conditions

3.1. Basic equations

The equations of motion for piezomagnetic materials without body force take the form

$$\frac{\partial\sigma_{x_1x_1}}{\partial x_1} + \frac{\partial\sigma_{x_1x_3}}{\partial x_3} = \rho\frac{\partial^2 u}{\partial t^2}, \tag{3}$$

$$\frac{\partial\sigma_{x_1x_3}}{\partial x_1} + \frac{\partial\sigma_{x_3x_3}}{\partial x_3} = \rho\frac{\partial^2 w}{\partial t^2}, \tag{4}$$

and Maxwell magnetostatic equation is

$$\frac{\partial B_{x_1}}{\partial x_1} + \frac{\partial B_{x_3}}{\partial x_3} = 0, \tag{5}$$

where σ_{mn} are stress components, u and w are the displacements, B_m are magnetic inductions, ρ is mass density and t is time variable.

The geometric equations are

$$[\varepsilon_{x_1x_1} \quad \varepsilon_{x_3x_3} \quad \varepsilon_{x_1x_3}]^T = \left[\frac{\partial u}{\partial x_1}\ \frac{\partial w}{\partial x_3}\ \frac{1}{2}\left(\frac{\partial u}{\partial x_3} + \frac{\partial w}{\partial x_1}\right)\right]^T, \tag{6}$$

and the Gauss equations are

$$[H_{x_1} \quad H_{x_3}]^T = \left[-\frac{\partial\psi}{\partial x_1} - \frac{\partial\psi}{\partial x_3}\right]^T, \tag{7}$$

where ε_{mn} are strains, H_m are magnetic fields, ψ is the magnetic potential and the superscript T means the transposition of a vector.

The constitutive equations for homogeneous piezomagnetic materials can be written as:

$$\begin{bmatrix}\delta\sigma_{x_1x_1}\\ \delta\sigma_{x_3x_3}\\ \delta B_{x_3}\end{bmatrix} = \begin{bmatrix}c_{11} & c_{13} & -d_{31}\\ c_{13} & c_{33} & -d_{33}\\ d_{31} & d_{33} & \mu_{33}\end{bmatrix}\begin{bmatrix}\delta\varepsilon_{x_1x_1}\\ \delta\varepsilon_{x_3x_3}\\ \delta H_{x_3}\end{bmatrix}, \tag{8}$$

$$\begin{bmatrix}\delta\sigma_{x_1x_3}\\ \delta B_{x_1}\end{bmatrix} = \begin{bmatrix}2c_{44} & -d_{15}\\ 2d_{15} & \mu_{11}\end{bmatrix}\begin{bmatrix}\delta\varepsilon_{x_1x_3}\\ \delta H_{x_1}\end{bmatrix}, \tag{9}$$

where the character "δ" represents small variations of the stresses, magnetic inductions, strains and magnetic fields about preexisting fields because of the magnetic status of the material (Giannakopoulos and Parmaklis, 2007), and will be dropped in the rest of the analysis for brevity.

3.2. Boundary conditions

To make the present time-related problem tractable, the Galilean transformation is introduced

$$x = x_1 + Vt, \quad z = x_3, \tag{10}$$

where the translating coordinate system (x,z) is attached to the moving punch. In the translating reference frame, the magnetoelastic quantities beneath the punch are assumed to be time invariant since the moving of the punch has prevailed for such a long time. In the following, boundary conditions in translating coordinate system (x,z) will be given. For the mechanical boundary conditions in translating coordinate system (x,z), one has

$$w(x,0) = \begin{cases} -w_0 & x\in[-a,a], \quad \textit{frictional flat}\\ -w_0 + x^2/2R, & x\in[-a,b], \quad \textit{frictional cylindrical}, \end{cases} \tag{11}$$

$$\sigma_{zz}(x,0) = -p(x), \qquad x \in [-a,b], \tag{12}$$

$$\sigma_{zz}(x,0) = 0, \quad x \notin [-a,b], \tag{13}$$

$$\sigma_{xz}(x,0) = -q(x), \quad x \in [-a,b], \tag{14}$$

$$\sigma_{xz}(x,0) = 0, \quad x \notin [-a,b], \tag{15}$$

where the penetration depth $w(x,0)$ is known beforehand, R denotes the radius of the frictional cylindrical punch. In Eqs. (12) and (14), $p(x)$ and $q(x)$ are, respectively, unknown surface contact stress and shear stress beneath the punch and satisfy the Coulomb friction law

$$q(x) = \mu_f p(x), \quad -a < x < b. \tag{16}$$

The equilibrium condition for the punch should be satisfied

$$\int_{-a}^{b} p(x)dx = P. \tag{17}$$

Note that in Eqs. (11)–(17) the contact region is denoted as $[-a,b]$ for various punch profiles for convenience.

For a perfectly magnetic insulating punch, one has

$$B_z(x,0) = 0, \quad |x| < \infty. \tag{18}$$

For semi-infinite piezomagnetic materials, the following regularity conditions apply:

$$u(x,z), w(x,z), \psi(x,z) \to 0, \quad \sqrt{x^2+z^2} \to \infty. \tag{19}$$

4. Formulation of the problem

In view of the Galilean transformation Eq. (10), one can obtain the following governing equations in terms of the principal physical quantities (u, w, ψ):

$$(c_{11} - c_{44}\cdot c^2)\frac{\partial^2 u}{\partial x^2} + c_{44}\frac{\partial^2 u}{\partial z^2} + (c_{13}+c_{44})\frac{\partial^2 w}{\partial x \partial z} + (d_{31}+d_{15})\frac{\partial^2 \psi}{\partial x \partial z} = 0, \tag{20}$$

$$c_{44}(1-c^2)\frac{\partial^2 w}{\partial x^2} + c_{33}\frac{\partial^2 w}{\partial z^2} + (c_{13}+c_{44})\frac{\partial^2 u}{\partial x \partial z} + d_{15}\frac{\partial^2 \psi}{\partial x^2} + d_{33}\frac{\partial^2 \psi}{\partial z^2} = 0, \tag{21}$$

$$d_{15}\frac{\partial^2 w}{\partial x^2} + d_{33}\frac{\partial^2 w}{\partial z^2} + (d_{15}+d_{31})\frac{\partial^2 u}{\partial x \partial z} - \mu_{11}\frac{\partial^2 \psi}{\partial x^2} - \mu_{33}\frac{\partial^2 \psi}{\partial z^2} = 0, \tag{22}$$

where $c = V/c_{sh}$ is the relative moving speed of the punch with $c_{sh} = \sqrt{c_{44}/\rho}$ being the shear wave speed.

4.1. Solution of the governing equations

The solutions of Eqs. (20)–(22) can be written as follows:

$$\begin{bmatrix} u \\ w \\ \psi \end{bmatrix} = \int_{-\infty}^{+\infty} \sum_{n=1}^{3} \begin{bmatrix} M_n^{(u)}(\omega,z) \\ M_n^{(w)}(\omega,z) \\ M_n^{(\psi)}(\omega,z) \end{bmatrix} C_n e^{-i\omega x} d\omega, \tag{23}$$

where $i^2 = -1$, ω is the Fourier variable, $C_n (n = 1,2,3)$ are unknown functions to be determined from the boundary conditions and $M_n^{(u)}(\omega,z)$, $M_n^{(w)}(\omega,z)$ and $M_n^{(\psi)}(\omega,z) (n = 1,2,3)$ are given as:

$$\begin{aligned} M_1^{(u)}(\omega,z) &= e^{|\omega|\tau_1 z}, \quad M_2^{(u)}(\omega,z) = \cos(|\omega|v_1 z)e^{|\omega|\mu_1 z}, \\ M_3^{(u)}(\omega,z) &= \sin(|\omega|v_1 z)e^{|\omega|\mu_1 z}, \end{aligned} \tag{24}$$

$$\begin{aligned} M_1^{(w)}(\omega,z) &= -i\cdot sign(\omega)\cdot \mathrm{H}_1(\tau_1)e^{|\omega|\tau_1 z}, \\ M_2^{(w)}(\omega,z) &= -i\cdot sign(\omega)[Re(\mathrm{H}_1(\tau_2))\cos(|\omega|v_1 z) \\ &\quad -\mathrm{Im}(\mathrm{H}_1(\tau_2))\sin(|\omega|v_1 z)]e^{|\omega|\mu_1 z}, \\ M_3^{(w)}(\omega,z) &= -i\cdot sign(\omega)[\mathrm{Im}(\mathrm{H}_1(\tau_2))\cos(|\omega|v_1 z) \\ &\quad +\mathrm{Re}(\mathrm{H}_1(\tau_2))\sin(|\omega|v_1 z)]e^{|\omega|\mu_1 z}, \end{aligned} \tag{25}$$

$$\begin{aligned} M_1^{(\psi)}(\omega,z) &= -i\cdot sign(\omega)\cdot \mathrm{H}_2(\tau_1)e^{|\omega|\tau_1 z}, \\ M_2^{(\psi)}(\omega,z) &= -i\cdot sign(\omega)[Re(\mathrm{H}_2(\tau_2))\cos(|\omega|v_1 z) \\ &\quad -\mathrm{Im}(\mathrm{H}_2(\tau_2))\sin(|\omega|v_1 z)]e^{|\omega|\mu_1 z}, \\ M_3^{(\psi)}(\omega,z) &= -i\cdot sign(\omega)[\mathrm{Im}(\mathrm{H}_2(\tau_2))\cos(|\omega|v_1 z) \\ &\quad +\mathrm{Re}(\mathrm{H}_2(\tau_2))\sin(|\omega|v_1 z)]e^{|\omega|\mu_1 z}, \end{aligned} \tag{26}$$

where $sign(\cdot)$ represents the sign function, $\mathrm{Re}(\cdot)$ and $\mathrm{Im}(\cdot)$ stand for the real part and imaginary part and the functions $\mathrm{H}_1(\cdot)$ and $\mathrm{H}_2(\cdot)$ are defined as:

$$\begin{aligned} \mathrm{H}_1(x) &= \frac{(c_{13}+c_{44})(d_{31}+d_{15})x^2 + \left[c_{44}x^2 - (c_{11}-c_{44}\cdot c^2)\right]\left(d_{33}x^2 - d_{15}\right)}{(c_{13}+c_{44})x(d_{33}x^2-d_{15}) - (d_{31}+d_{15})x\left[c_{33}x^2 - c_{44}(1-c^2)\right]}, \\ \mathrm{H}_2(x) &= -\frac{\left[c_{44}x^2 - (c_{11}-c_{44}\cdot c^2)\right]\left[c_{33}x^2 - c_{44}(1-c^2)\right] + (c_{13}+c_{44})^2 x^2}{(c_{13}+c_{44})x(d_{33}x^2-d_{15}) - (d_{31}+d_{15})x\left[c_{33}x^2 - c_{44}(1-c^2)\right]}, \end{aligned} \tag{27}$$

where τ_1 and $\tau_2 = \mu_1 + iv_1$ plus $\tau_3 = \mu_1 - iv_1$ are the roots of the following characteristic equation related to governing equations Eqs. (20)–(22) with consideration of Eq. (2):

$$\begin{vmatrix} c_{44}\tau^2 - (c_{11} - c_{44}\cdot c^2) & -i\cdot sign(\omega)(c_{13}+c_{44})\tau & -i\cdot sign(\omega)(d_{31}+d_{15})\tau \\ -i\cdot sign(\omega)(c_{13}+c_{44})\tau & c_{33}\tau^2 - c_{44}(1-c^2) & d_{33}\tau^2 - d_{15} \\ -i\cdot sign(\omega)(d_{31}+d_{15})\tau & d_{33}\tau^2 - d_{15} & \mu_{11} - \mu_{33}\tau^2 \end{vmatrix} = 0. \tag{28}$$

In the present model, the dynamic motion should be subsonic (i.e. the moving speed V is below the shear wave speed $c_{sh} = \sqrt{c_{44}/\rho}$) on considering the regularity conditions Eq. (19) involving semi-infinite materials, which require that three roots of the totally six roots of characteristic equation Eq. (28) have positive real part. Thus $0 \leqslant c < 1$.

It deserves noting that the terms $|\omega|$ and $sign(\omega)$ in Eqs. (24)–(26) benefit the changes of the Fourier domain from $[-\infty,\infty]$ to $[0,\infty]$, which enable one to get the singular integral equation of the second kind as will be seen later.

It is clearly found that the characteristic roots of Eq. (28) is dependent on the relative sliding speed c since the inertial terms in equations of motion, Eqs. (3) and (4), are considered and Galilean transformation, Eq. (10), is utilized. Thus, relative sliding speed c may affect the contact behavior in the present moving contact model for piezomagnetic materials.

4.2. Determination of the unknown functions

As mentioned above, in Eq. (23), unknown functions $C_n (n = 1,2,3)$ need to be determined from the boundary conditions. Considering Eqs. (23) and (8)–(10) and using boundary conditions Eqs. (12)–(15) and (18) yield the following expressions for unknown functions $C_n (n = 1,2,3)$:

$$C_n = \frac{(-1)^n}{|\omega| D_{coe}}\left[\Gamma_1(\omega)D_{1n} - \Gamma_2(\omega)D_{2n}\right] \quad (n = 1,2,3), \tag{29}$$

where D_{coe} is the determinant of matrix (a_{mn}) $(m, n = 1,2,3)$, which is given in Appendix A, $D_{mn}(m, n = 1,2,3)$ is the determinant of the same matrix corresponding to the elimination of the mth row and nth column and $\Gamma_1(\omega)$ and $\Gamma_2(\omega)$ are given as follows:

$$\Gamma_1(\omega) = \frac{1}{2\pi}\int_{-a}^{b} p(\xi)e^{i\omega\xi}d\xi, \quad \Gamma_2(\omega) = \frac{1}{2\pi}\int_{-a}^{b} q(\xi)e^{i\omega\xi}d\xi. \tag{30}$$

4.3. Integral equation

Differentiating the second equation of Eq. (23) on the surface and using Eqs. (29) and (30) produce an integral equation as follows:

$$\frac{\partial w(x,0)}{\partial x}=\frac{1}{\pi}\int_{-a}^{b}\int_{0}^{\infty}K_1\sin[\omega(\xi-x)]p(\xi)d\omega d\xi+\frac{1}{\pi}\int_{-a}^{b}\int_{0}^{\infty}K_2\cos[\omega(\xi-x)]q(\xi)d\omega d\xi,\quad |x|<\infty, \tag{31}$$

where

$$\begin{aligned}K_1&=\sum_{n=1}^{3}(-1)^n M_n^{(w)}(\omega,0)\tfrac{D_{1n}}{D_{coe}},\\ K_2&=i\sum_{n=1}^{3}(-1)^n M_n^{(w)}(\omega,0)\tfrac{D_{2n}}{D_{coe}}\end{aligned}. \tag{32}$$

Noting that K_1 and K_2 are independent of the Fourier variable ω, one can recast Eq. (31) to the following singular integral equation of the second kind:

$$\frac{\partial w(x,0)}{\partial x}=K_2 q(x)+\frac{1}{\pi}\int_{-a}^{b}\frac{K_1}{\xi-x}p(\xi)d\xi,\quad |x|<\infty. \tag{33}$$

In obtaining Eq. (33), the following relations are used:

$$\begin{aligned}&\int_0^\infty \sin[\omega(\xi-x)]d\omega=\frac{1}{\xi-x},\\ &\int_0^\infty \cos[\omega(\xi-x)]d\omega=\pi\delta(\xi-x),\end{aligned} \tag{34}$$

where $\delta(\cdot)$ is the Dirac delta function.

4.4. General expressions of the surface in-plane stress and magnetic induction

On getting the solution of Eq. (31) and the equilibrium condition (17), the surface in-plane stress and magnetic induction, which have a quantity of physical interest, can be written as:

$$\sigma_{xx}(x,0)=\frac{1}{\pi}\int_{-a}^{b}\int_{0}^{\infty}\Delta_{11}\cos[\omega(\xi-x)]p(\xi)d\omega d\xi+\frac{1}{\pi}\int_{-a}^{b}\int_{0}^{\infty}\Delta_{12}\sin[\omega(\xi-x)]q(\xi)d\omega d\xi,\quad |x|<\infty, \tag{35}$$

$$B_x(x,0)=\frac{1}{\pi}\int_{-a}^{b}\int_{0}^{\infty}\Delta_{21}\sin[\omega(\xi-x)]p(\xi)d\omega d\xi+\frac{1}{\pi}\int_{-a}^{b}\int_{0}^{\infty}\Delta_{22}\cos[\omega(\xi-x)]q(\xi)d\omega d\xi,\quad |x|<\infty, \tag{36}$$

where

$$\begin{aligned}\Delta_{11}&=\sum_{n=1}^{3}(-1)^n \mathrm{T}_{1n}\tfrac{D_{1n}}{D_{coe}},\quad \Delta_{12}=i\sum_{n=1}^{3}(-1)^{n+1}\mathrm{T}_{1n}\tfrac{D_{2n}}{D_{coe}},\\ \Delta_{21}&=i\sum_{n=1}^{3}(-1)^n \mathrm{T}_{2n}\tfrac{D_{1n}}{D_{coe}},\quad \Delta_{22}=\sum_{n=1}^{3}(-1)^{n+1}\mathrm{T}_{2n}\tfrac{D_{2n}}{D_{coe}},\end{aligned} \tag{37}$$

where $\mathrm{T}_{kn}(k=1,2,n=1,2,3)$ are given in Appendix A.

It is noted that in Eqs. (31), (35), and (36), the Fourier domain is changed to $[0,\infty]$ from $[-\infty,\infty]$ by using the odd or even properties of the kernels of the corresponding integral equations in terms of the Fourier variable ω.Eqs. (35) and (36) can further be rewritten as:

$$\sigma_{xx}(x,0)=\Delta_{11}p(x)+\frac{1}{\pi}\int_{-a}^{b}\frac{\Delta_{12}}{\xi-x}q(\xi)d\xi,\quad |x|<\infty, \tag{38}$$

$$B_x(x,0)=\Delta_{22}q(x)+\frac{1}{\pi}\int_{-a}^{b}\frac{\Delta_{21}}{\xi-x}p(\xi)d\xi,\quad |x|<\infty. \tag{39}$$

5. Exact solutions for a frictional moving flat punch

Considering the first condition of Eq. (11) and using Eq. (16), one can normalize Eq. (31) and the equilibrium condition (17) as:

$$K_2\cdot\mu_f\cdot\chi(t)+\frac{1}{\pi}\int_{-1}^{1}\frac{K_1}{r-t}\chi(r)dr=0,\quad |t|<1, \tag{40}$$

$$\int_{-1}^{1}\chi(r)dr=\frac{P}{a}, \tag{41}$$

where the following variable transformations have been utilized:

$$x=at,\quad \xi=ar,\quad p(x)=\chi(t). \tag{42}$$

The index of the singular integral equation Eq. (40) is

$$\kappa_0=-(\alpha+\beta)=1, \tag{43}$$

where α and β take the following form:

$$\begin{aligned}&\zeta>0:\ \alpha=-\tfrac{\theta}{\pi},\quad \beta=\tfrac{\theta}{\pi}-1,\\ &\zeta=0:\ \alpha=-\tfrac{1}{2},\quad \beta=-\tfrac{1}{2},\\ &\zeta<0:\ \alpha=\tfrac{\theta}{\pi}-1,\quad \beta=-\tfrac{\theta}{\pi},\end{aligned} \tag{44}$$

where

$$\zeta=\frac{\mu_f K_2}{K_1},\quad \tan\theta=\left|\frac{1}{\zeta}\right|. \tag{45}$$

Thus, the solution to Eqs. (40) and (41) can be expressed in terms of Jacobi Polynomials $P_m^{(\alpha,\beta)}(\cdot)$ as (Erdogan, 1978):

$$\chi(t)=\varpi(t)\sum_{m=0}^{\infty}\eta_m P_m^{(\alpha,\beta)}(t),\quad |t|<1, \tag{46}$$

with weight function $\omega(t)$ defined as:

$$\varpi(t)=(1-t)^{\alpha}(1+t)^{\beta},\quad |t|<1, \tag{47}$$

where $\eta_m(m\geqslant 0)$ are unknown coefficients to be determined.

Inspecting the linear independence of the Jacobi Polynomials $P_m^{(\alpha,\beta)}(\cdot)$ and defining

$$\sigma_0=\frac{P}{2a}, \tag{48}$$

one can get the only nonzero coefficient η_0

$$\eta_0=-\frac{2\sigma_0\sin(\pi\alpha)}{\pi}. \tag{49}$$

Thus, the surface contact stress in physical coordinates can be obtained as:

$$p(x)=-\frac{2\sigma_0\sin(\pi\tau)}{\pi}\left(1-\frac{x}{a}\right)^{\alpha}\left(1+\frac{x}{a}\right)^{\beta},\quad |x|<a. \tag{50}$$

The mode I stress intensity factor at the edges of the flat punch can be defined as:

$$S_I(a)=\lim_{x\to a}\frac{p(x)}{2^{\beta}}(a-x)^{-\alpha}=\frac{\eta_0}{a^{\alpha}}, \tag{51}$$

$$S_I(-a)=\lim_{x\to -a}\frac{p(x)}{2^{\alpha}}(a+x)^{-\beta}=\frac{\eta_0}{a^{\beta}}. \tag{52}$$

Setting $\mu_f=0$ leads to the following simplified expression for Eqs. (51) and (52):

$$S_I(a)=S_I(-a)=\eta_0\sqrt{a}=\frac{P}{\pi\sqrt{a}}. \tag{53}$$

The closed-form expressions of the surface in-plane stress and magnetic induction given in Eqs. (38) and (39) are obtained as (Guler and Erdogan, 2004):

$$\sigma_{xx}(x,0) = -\frac{2\sigma_0 \sin(\pi\alpha)}{\pi} \times \begin{cases} \Delta_{11}\left(1-\frac{x}{a}\right)^{\alpha}\left(1+\frac{x}{a}\right)^{\beta} + \frac{\Delta_{12}\cdot\mu_f}{\pi}\Lambda_F(x), & |x|<a \\ \frac{\Delta_{12}\cdot\mu_f}{\pi}\Lambda_F(x), & |x|>a \end{cases}, \tag{54}$$

$$B_x(x,0) = -\frac{2\sigma_0 \sin(\pi\alpha)}{\pi} \times \begin{cases} \Delta_{22}\cdot\mu_f\left(1-\frac{x}{a}\right)^{\alpha}\left(1+\frac{x}{a}\right)^{\beta} + \frac{\Delta_{21}}{\pi}\Lambda_F(x), & |x|<a \\ \frac{\Delta_{21}}{\pi}\Lambda_F(x), & |x|>a \end{cases}, \tag{55}$$

where $\Lambda_F(x)$ is given as:

$$\Lambda_F(x) = \frac{\pi}{\sin(\pi\alpha)} \begin{cases} -\left(1-\frac{x}{a}\right)^{\alpha}\left(-\frac{x}{a}-1\right)^{\beta}, & x<-a \\ \left(1-\frac{x}{a}\right)^{\alpha}\left(1+\frac{x}{a}\right)^{\beta}\cos(\pi\alpha), & -a<x<a \\ \left(\frac{x}{a}-1\right)^{\alpha}\left(1+\frac{x}{a}\right)^{\beta}, & x>a \end{cases}. \tag{56}$$

Especially, when friction coefficient $\mu_f = 0$, the surface contact stress (50) becomes

$$p(x) = \frac{P}{\pi\sqrt{a^2-x^2}}, \quad |x|<a. \tag{57}$$

This formula is just the same as Eq. (56) for frictionless contact problem involving piezomagnetic materials given by Zhou and Lee (2012), which justifies our derivation for a frictional flat punch.

6. Exact solutions for a frictional moving cylindrical punch

Considering the second condition of Eq. (11) and using Eq. (16), one can normalize Eq. (31) and the equilibrium condition (17) as:

$$K_2\cdot\mu_f\cdot\chi(t) + \frac{1}{\pi}\int_{-1}^{1}\frac{K_1}{r-t}\chi(r)dr = \frac{\lambda_1 t+\lambda_2}{2R}, \quad |t|<1, \tag{58}$$

$$\int_{-1}^{1}\chi(r)dr = \frac{2P}{\lambda_1}, \tag{59}$$

where

$$\lambda_1 = b+a, \quad \lambda_2 = b-a, \tag{60}$$

and the following variable transformations have been utilized:

$$x = \frac{\lambda_1}{2}t+\frac{\lambda_2}{2}, \quad \xi = \frac{\lambda_1}{2}r+\frac{\lambda_2}{2}, \quad p(x)=\chi(t). \tag{61}$$

The index of the singular integral equation Eq. (58) is

$$\kappa_0 = -(\alpha+\beta) = -1, \tag{62}$$

where α and β take the following form:

$$\begin{aligned} &\zeta>0: \alpha = 1-\tfrac{\theta}{\pi}, \quad \beta = \tfrac{\theta}{\pi}, \\ &\zeta=0: \alpha = \tfrac{1}{2}, \quad \beta = \tfrac{1}{2}, \\ &\zeta<0: \alpha = \tfrac{\theta}{\pi}, \quad \beta = 1-\tfrac{\theta}{\pi}, \end{aligned} \tag{63}$$

where ζ is the same as that given in Eq. (45).

The solution to Eqs. (58) and (59) can also be expressed in terms of Jacobi Polynomials $P_m^{(\alpha,\beta)}(\cdot)$ as the same as given in Eq. (46) with weight function $\omega(t)$ defined in Eq. (47).

Since $\kappa_0 = -(\alpha+\beta) = -1$, in addition of Eq. (59), the following consistency condition must be fulfilled:

$$\int_{-1}^{1}\frac{1}{\varpi(t)}\frac{\lambda_1 t+\lambda_2}{2R}dt = 0. \tag{64}$$

Using the Jacobi Polynomials $P_m^{(\alpha,\beta)}(\cdot)$, one can find the only non-zero coefficient

$$\eta_0 = \frac{\lambda_1}{-2\cdot K_1\cdot R}\sin(\pi\alpha). \tag{65}$$

Substituting Eq. (65) into Eq. (46) and then Eq. (59), one can obtain the following relationship between the applied load and the contact length:

$$P = \frac{\pi\cdot\alpha\cdot\beta}{-2\cdot K_1\cdot R}(\lambda_1)^2. \tag{66}$$

Moreover, Substituting Eq. (65) into the consistency condition Eq. (64), one obtains

$$b = \frac{\beta}{\alpha}a. \tag{67}$$

Considering Eqs. (66) and (67), one can finally determine the unknown contact region under a cylindrical punch.

The surface contact stress, in-plane stress and magnetic induction can be given as (Guler and Erdogan, 2007):

$$p(x) = -\frac{\sin(\pi\alpha)}{K_1\cdot R}(b-x)^{\alpha}(x+a)^{\beta}, \quad -a<x<b, \tag{68}$$

$$\sigma_{xx}(x,0) = \frac{\sin(\pi\alpha)}{-K_1\cdot R}\begin{cases}\Delta_{11}(b-x)^{\alpha}(x+a)^{\beta} + \frac{\Delta_{12}\cdot\mu_f}{2\pi}\Lambda_c(x), & -a<x<b \\ \frac{\Delta_{12}\cdot\mu_f}{2\pi}\Lambda_c(x), & x\notin[-a,b]\end{cases}, \tag{69}$$

$$B_x(x,0) = \frac{\sin(\pi\alpha)}{-K_1\cdot R}\begin{cases}\Delta_{22}\cdot\mu_f(b-x)^{\alpha}(x+a)^{\beta} + \frac{\Delta_{21}}{2\pi}\Lambda_c(x), & -a<x<b \\ \frac{\Delta_{21}}{2\pi}\Lambda_c(x), & x\notin[-a,b]\end{cases}, \tag{70}$$

where $\Lambda_c(x)$ is given as

$$\Lambda_c(x) = \frac{\pi}{\sin(\pi\alpha)} \begin{cases} -2(b-x)^{\alpha}(-x-a)^{\beta} - 2x + b - a + (\alpha-\beta)(b+a), & x<-a \\ 2(b-x)^{\alpha}(x+a)^{\beta} - 2x + b - a + (\alpha-\beta)(b+a), & -a<x<b \\ 2(x-b)^{\alpha}(x+a)^{\beta} - 2x + b - a + (\alpha-\beta)(b+a), & x>b \end{cases}. \tag{71}$$

Especially, when friction coefficient $\mu_f = 0$, the surface contact stress (68) becomes

$$p(x) = -\frac{\sqrt{a^2-x^2}}{K_1\cdot R}, \quad |x|<a. \tag{72}$$

This formula is just the same as Eq. (63) for frictionless contact problem involving piezomagnetic materials given by Zhou and Lee (note the counterpart of $-K_1$ is L_1 in Zhou and Lee (2012)), which justifies our derivation for a frictional cylindrical punch.

7. Numerical results and discussions

Terfenol-D is selected among piezomagnetic materials in numerical computation to reveal the influences of the friction coefficient μ_f and the relative moving speed of the punch c on the contact behaviors. As discussed in Section 4, in the present model involving semi-infinite materials, the dynamic steady-state motion should be subsonic. Thus, c remains in the interval $[0, 1)$ in the numerical computation.

7.1. Contact behaviors under a frictional moving flat punch

Figs. 1 and 2, respectively, delineate the influences of the friction coefficient μ_f and the relative moving speed of the punch c

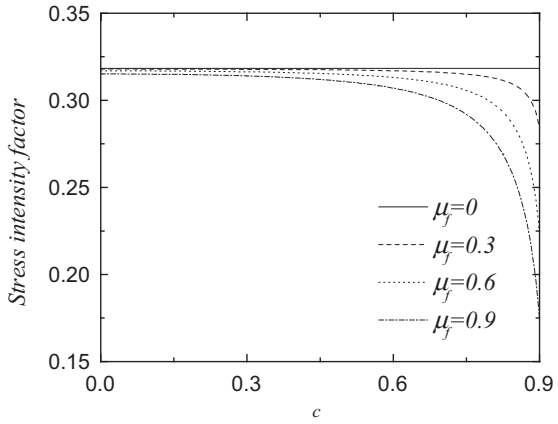

Fig. 1. Normalized stress intensity factors $S_I(a)/S_{01}$ and $S_I(-a)/S_{02}$ at the edges of the frictional flat punch for different values of the friction coefficient μ_f.

on the normalized stress intensity factors $S_I(a)/S_{01}$ and $S_I(-a)/S_{02}$, where $S_{01} = Pa^{\beta}$ and $S_{02} = Pa^{\alpha}$. It is observed that the normalized stress intensity factors are the same at both edges of the flat punch because after the normalization, $S_I(a)/S_{01} = S_I(-a)/S_{02} = -\sin(\pi\alpha)/\pi$. When the friction coefficient equals zero, the stress intensity factor keeps a constant, which may show validity of the present program. The relative moving speed of the punch c has no influence on the stress intensity factor when $\mu_f = 0$, which is reasonable, since smooth moving occurs.

In addition, Fig. 1 shows that the normalized stress intensity factors can be lowered by either of the following way: (i) escalating the moving speed of the punch or (ii) applying a bigger friction coefficient, which can be explained through considering Eqs. (44) and (45). Fig. 2 again confirms these conclusions.

Figs. 3 and 4 show the surface normal stress $\sigma_{zz}(x, 0)/\sigma_0(\sigma_0 = P/2a)$ distributions for different values of the friction coefficient μ_f and the relative moving speed of the punch c under a frictional moving flat punch. As expected, because of the singularity, $\sigma_{zz}(x, 0)$ becomes unbounded near both the trailing ($x = a$) and leading ($x = -a$) edges of the frictional flat punch. Thus, there are stress concentrations around both edges. Stress concentrations around the trailing edge are greater than those around the leading edge because α and β, powers of stress singularity at the trailing and leading edges, always hold the relationship $|\alpha| > |\beta|$. This concentration result is the same as that for the purely elastic material (Guler and Erdogan, 2004). These concentrations of surface normal

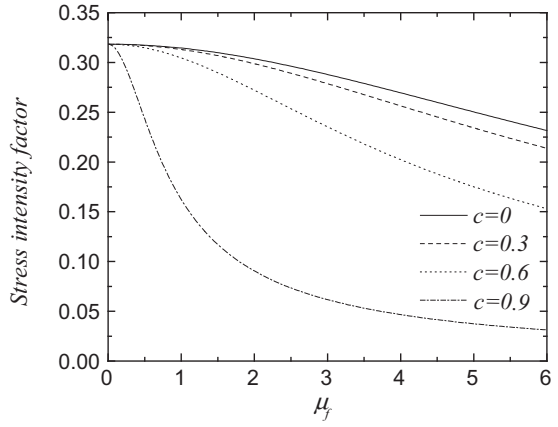

Fig. 2. Normalized stress intensity factors $S_I(a)/S_{01}$ and $S_I(-a)/S_{02}$ at the edges of the frictional flat punch for different values of the relative moving speed of the punch c.

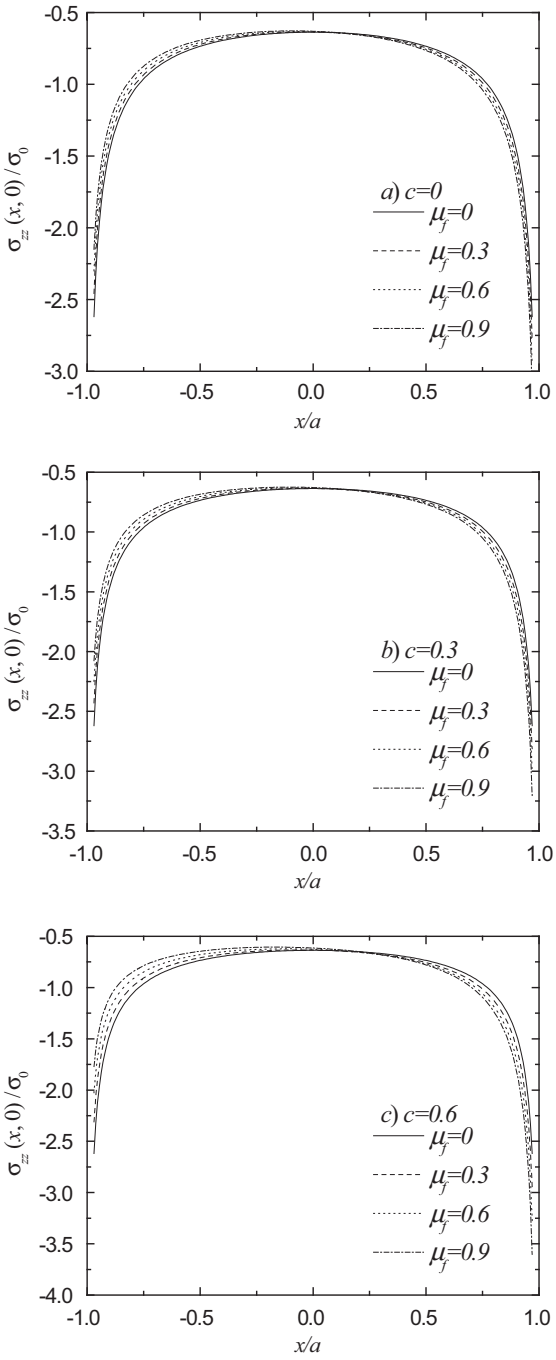

Fig. 3. The surface normal stress $\sigma_{zz}(x, 0)/\sigma_0$ distributions for different values of the friction coefficient μ_f under a frictional moving flat punch, (a) $c = 0$, (b) $c = 0.3$ and (c) $c = 0.6$.

stress at both edges may explain why the surface damage occurs in piezomagnetic materials.

It can be further inferred from Fig. 3 that the increasing of the friction coefficient results in intensifying the contact stress around the trailing edge, while lowering the contact stress around the leading edge. Since the punch moves smoothly, i.e. $\mu_f = 0$, the relative moving speed of the punch c does not affect the surface normal stress distribution as can be seen from Figs. 3 and 4(a), which is in accordance with results obtained in Fig. 1 that the relative moving speed of the punch c has no influence on the stress intensity factor when $\mu_f = 0$. In addition, the

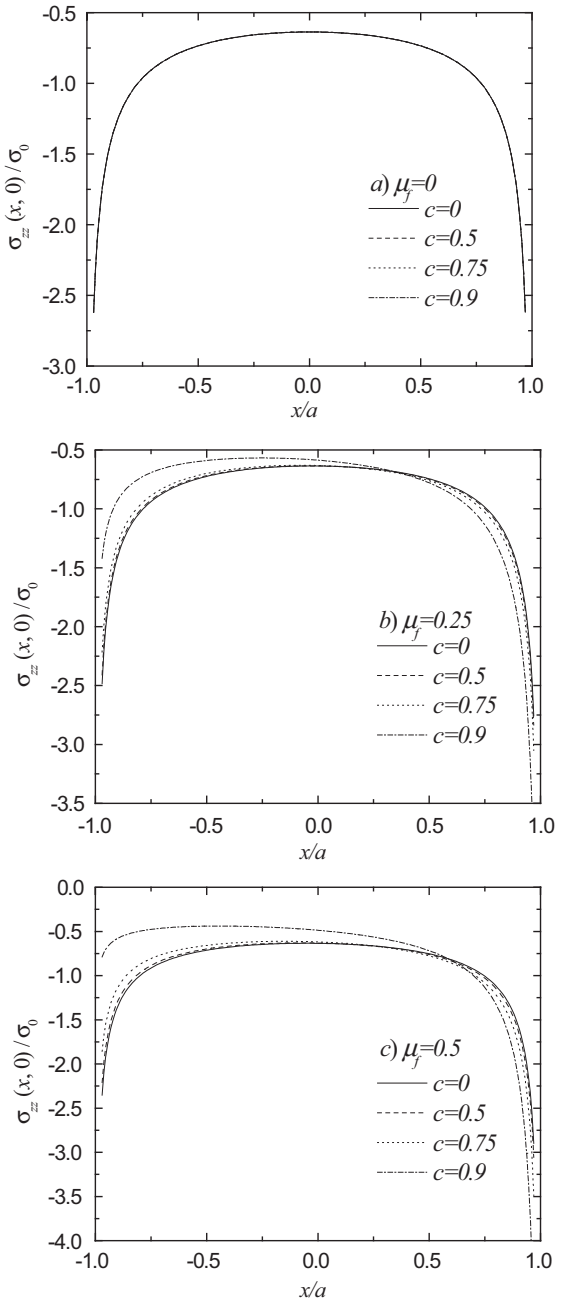

Fig. 4. The surface normal stress $\sigma_{zz}(x,0)/\sigma_0$ distributions for different values of the relative moving speed of the punch c under a frictional moving flat punch, (a) $\mu_f = 0$, (b) $\mu_f = 0.25$ and (c) $\mu_f = 0.5$.

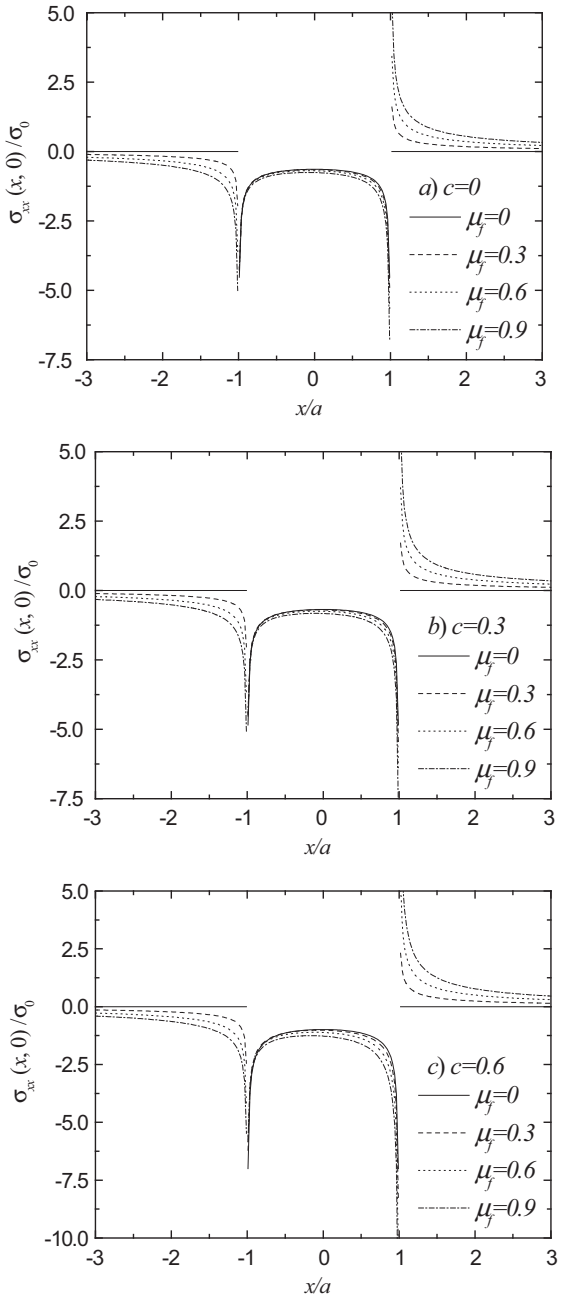

Fig. 5. The surface in-plane stress $\sigma_{xx}(x,0)/\sigma_0$ distributions for different values of the friction coefficient μ_f under a frictional moving flat punch, (a) $c = 0$, (b) $c = 0.3$ and (c) $c = 0.6$.

corresponding curves in Figs. 3 and 4(a) when the friction coefficient $\mu_f = 0$ are symmetric, which show the validity of the present program for a frictional flat punch. For the enlarged nonzero value of the friction coefficient, the contact stress concentrations around the trailing edge become bigger, while the opposite trend is seen around the leading edge as can be seen from Fig. 4(b) and (c).

The distributions of the surface in-plane stress $\sigma_{xx}(x,0)/\sigma_0(\sigma_0 = P/2a)$ for different values of the friction coefficient μ_f and the relative moving speed of the punch c under a frictional moving flat punch are plotted in Figs. 5 and 6. Figs. 5 and 6 clearly depict that the surface in-plane stress magnitude is unbounded and discontinuous at both edges of the frictional flat punch, which contributes the surface damage for piezomagnetic materials. Thus, the surface in-plane stress has a great practical interest in revealing the surface damage mechanism.

Fig. 5 also shows that the surface in-plane stress before the leading edge ($x < -a$) becomes more compressive, but more tensile behind the trailing edge ($x > a$) as the friction coefficient increases. When $\mu_f = 0$, the surface in-plane stress outside the contact region remains zero no matter how fast the punch moves. As can be seen from Fig. 5(b) and (c), the surface in-plane stress behind the trailing edge ($x > a$) is usually rendered more tensile, but more compressive in the remaining region of the Terfenol-D surface ($x < a$) with the punch moving faster for lower value c. When c becomes larger, for example, $0.9 \leqslant c < 1$, the surface in-plane stress insider the contact region tends to be tensile. Thus, one may conclude that

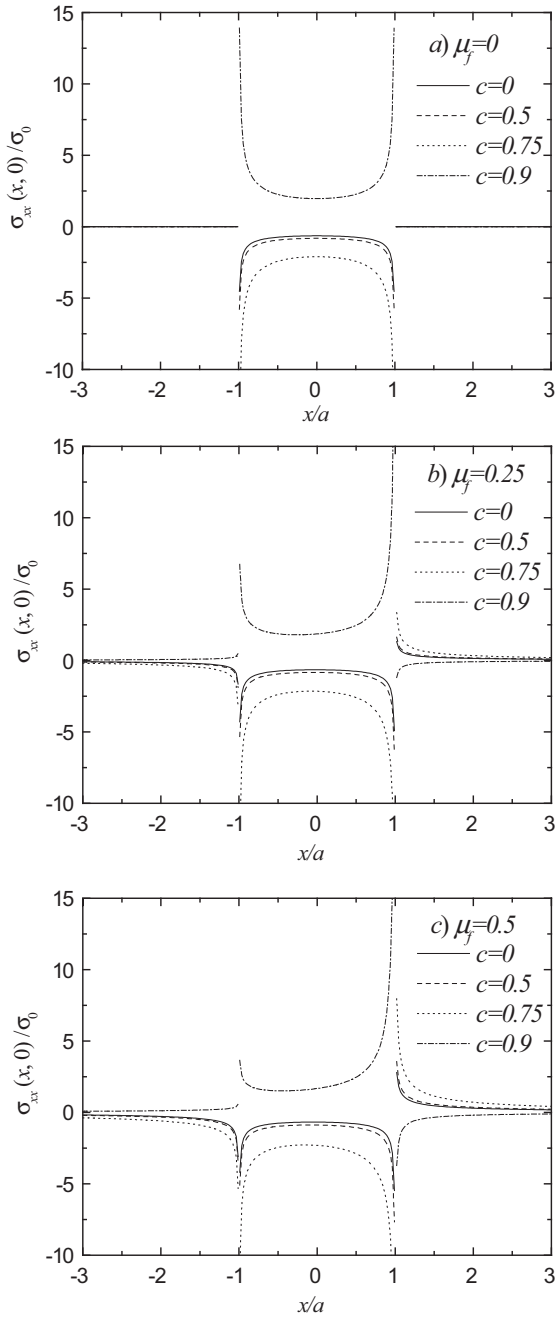

Fig. 6. The surface in-plane stress $\sigma_{xx}(x,0)/\sigma_0$ distributions for different values of the relative moving speed of the punch c under a frictional moving flat punch, (a) $\mu_f = 0$, (b) $\mu_f = 0.25$ and (c) $\mu_f = 0.5$.

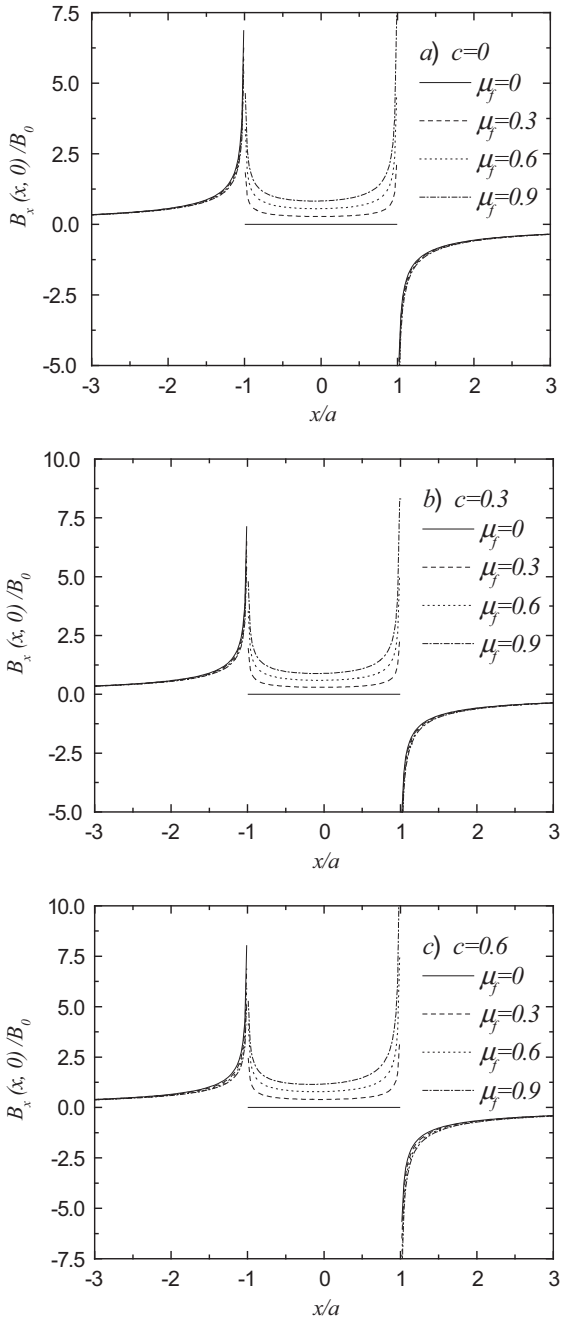

Fig. 7. The surface magnetic induction $B_x(x,0)/B_0$ distributions for different values of the friction coefficient μ_f under a frictional moving flat punch, (a) $c = 0$, (b) $c = 0.3$ and (c) $c = 0.6$.

when moving speed reaches a high moving speed, the surface in-plane stress inside the contact region becomes tensile from compressive values since the punch and piezomagnetic materials have great potential to be out of contact for a high moving speed approximating the lowest shear wave speed. It is predictable that the trailing edge is a more likely location of surface damage, possibly leading to surface crack initiation and propagation.

Figs. 7 and 8 examine the influences of the friction coefficient μ_f and the relative moving speed of the punch c on the surface magnetic induction $B_x(x,0)/B_0$ ($B_0 = d_{33}P/(2ac_{33})$) under a frictional moving flat punch. Like the surface in-plane stress case, the surface magnetic induction magnitude is also unbounded and discontinuous at both edges of the flat punch. Somewhat different from the surface in-plane stress case, the surface magnetic induction keeps positive when $x < a$, while negative when $x > a$. Quietly different from the purely elastic materials, for piezomagnetic materials, singularity of the surface magnetic induction at both edges also accounts for the surface damage besides singularities of the surface normal stress and in-plane stress.

Figs. 7 and 8 also demonstrate that the surface magnetic induction inside the contact region ($x < |a|$) becomes more positive with either the surface between Terfenol-D and the flat punch becoming more frictional or the punch moving faster. Additional result is that when the punch moves smoothly, i.e. $\mu_f = 0$, the surface magnetic induction remains zero inside the contact region ($x < |a|$), which may show that the surface magnetic induction inside the contact region is frictionally generated.

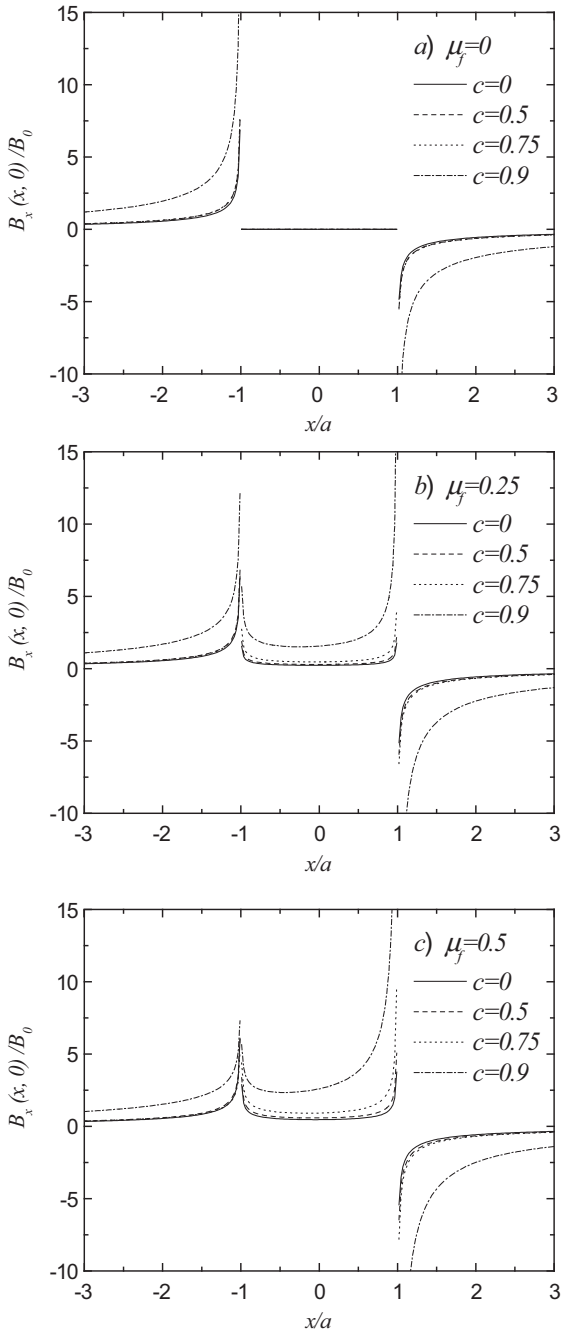

Fig. 8. The surface magnetic induction $B_x(x,0)/B_0$ distributions for different values of the relative moving speed of the punch c under a frictional moving flat punch, (a) $\mu_f = 0$, (b) $\mu_f = 0.25$ and (c) $\mu_f = 0.5$.

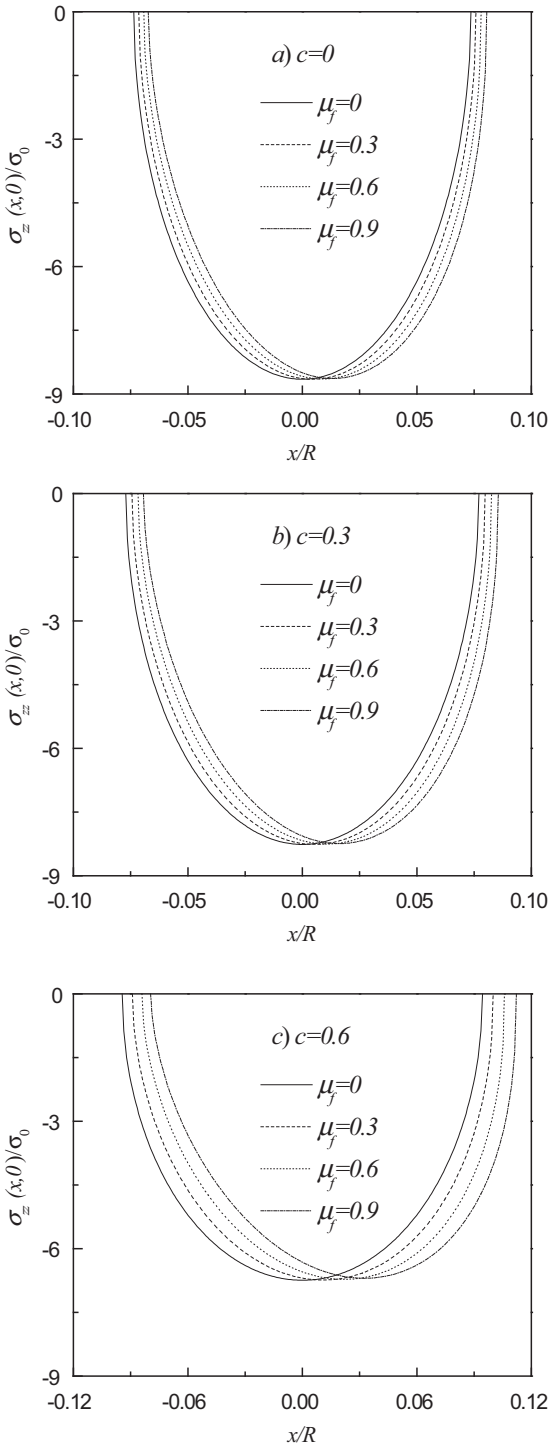

Fig. 9. The surface normal stress $\sigma_{zz}(x,0)/\sigma_0$ distributions for different values of the friction coefficient μ_f under a frictional moving cylindrical punch, (a) $c = 0$, (b) $c = 0.3$ and (c) $c = 0.6$.

Figs. 4, 6 and 8 demonstrate that the surface normal stress, surface in-plane stress and surface magnetic induction change a lot when c becomes larger than 0.5, while they do not change much when c varies between 0 and 0.5. Thus, there may exist a critical value c_0 for the relative moving speed of the punch c in dynamic contact problem under a frictional flat punch. When $c \in [0, c_0]$, c has an insignificant influence on the contact behaviors; while $c > c_0$, the influence of c on the contact behaviors becomes greater. In the present model involving piezomagnetic materials, $c \approx 0.5$.

7.2. Contact behaviors under a frictional moving cylindrical punch

Figs. 9 and 10 illustrate the influences of the friction coefficient μ_f and the relative moving speed of the punch c on the surface normal stress $\sigma_{zz}(x,0)/\sigma_0(\sigma_0 = P/R)$ under a frictional moving cylindrical punch. Different from the flat punch case, the surface normal stress is smooth at both edges of the cylindrical punch. The corresponding curves in Figs. 9 and 10 a) when the friction coefficient $\mu_f = 0$ are symmetric, which shows the validity of the present program for a frictional cylindrical punch. Furthermore, when the punch moves smoothly, the surface normal stress gets its maximum at the cylindrical punch center, which is the same as

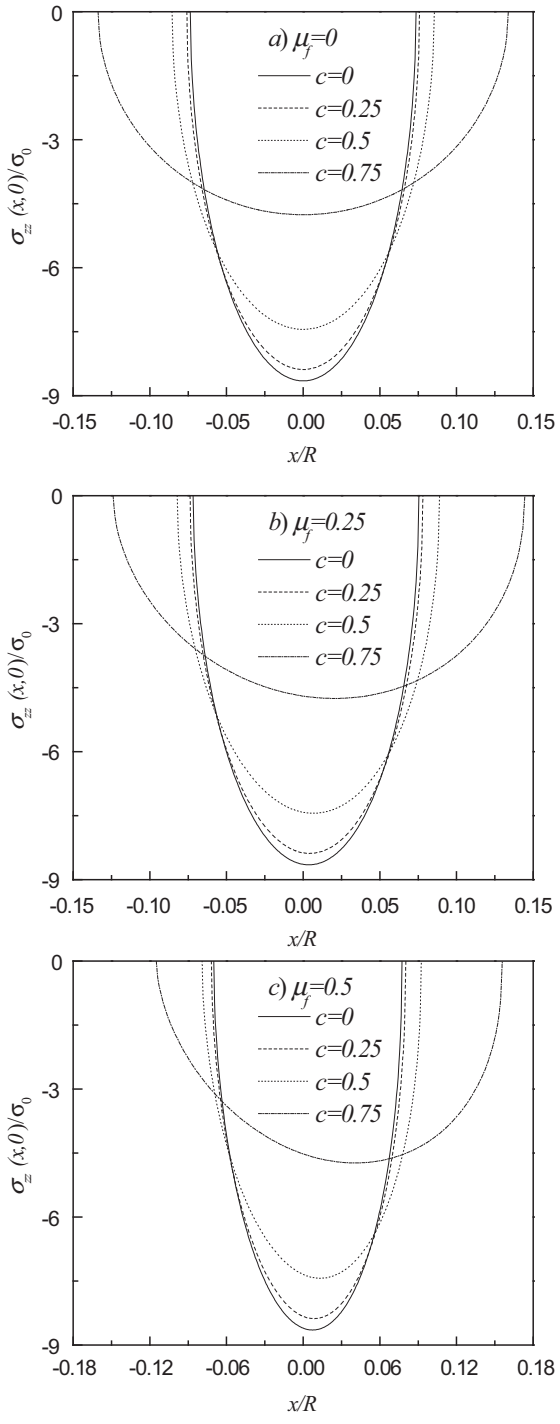

Fig. 10. The surface normal stress $\sigma_{zz}(x,0)/\sigma_0$ distributions for different values of the relative moving speed of the punch c under a frictional moving cylindrical punch, (a) $\mu_f = 0$, (b) $\mu_f = 0.25$ and (c) $\mu_f = 0.5$.

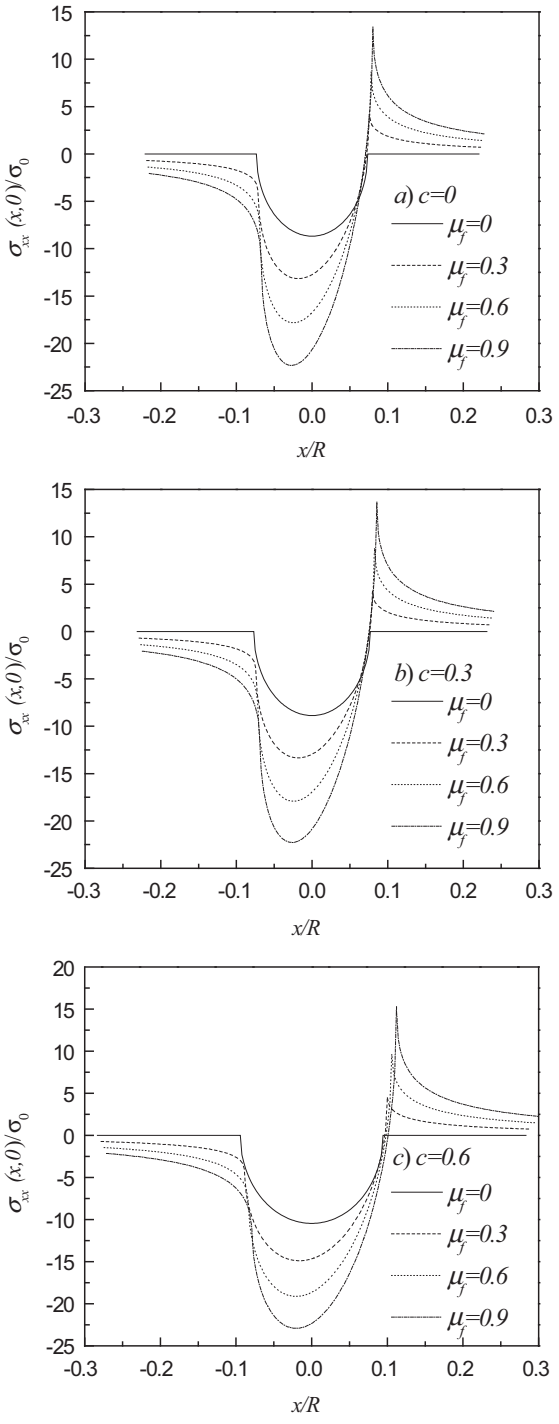

Fig. 11. The surface in-plane stress $\sigma_{xx}(x,0)/\sigma_0$ distributions for different values of the friction coefficient μ_f under a frictional moving cylindrical punch, (a) $c = 0$, (b) $c = 0.3$ and (c) $c = 0.6$.

the classic result on smooth contact for purely elastic materials. With either the nonzero value of the friction coefficient or the moving speed of the punch increasing, the position, where the peak magnitude value of the surface normal stress appears, becomes closer to the edge $x = b$ since the nominal powers of stress singularity have the relationship $\beta > \alpha > 0$.

Unlike the flat punch case, the contact region under the frictional cylindrical punch is unknown a priori, which can be determined from Eqs. (66) and (67). Figs. 9 and 10 demonstrate that the contact region enlarges ether as the friction coefficient μ_f increases or as the frictional cylindrical punch moves faster. In the preset dynamic frictional contact model, the moving speed of the punch does affect the width of the contact region and the influence becomes great when c reaches a larger value.

The variations of the surface in-plane stress $\sigma_{xx}(x,0)/\sigma_0(\sigma_0 = P/R)$ for different values of the friction coefficient μ_f and the relative moving speed of the punch c under a frictional moving cylindrical punch are examined in Figs. 11 and 12. The surface in-plane stress has a tensile spike at the edge $x = b$, whose value may increase with

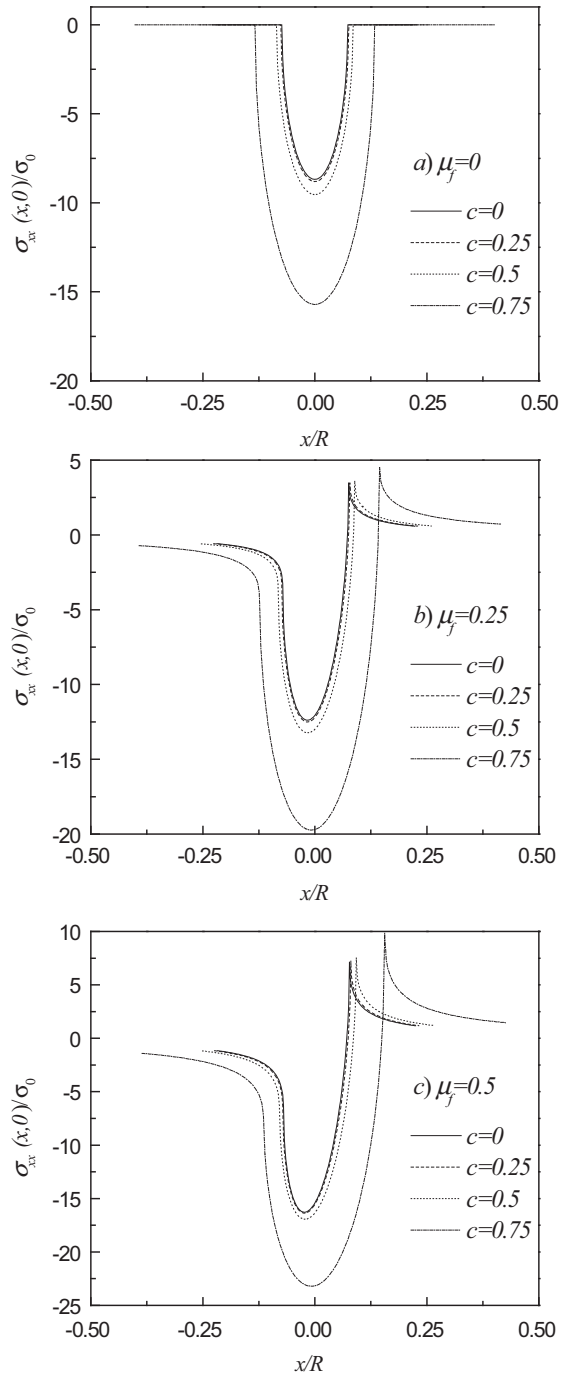

Fig. 12. The surface in-plane stress $\sigma_{xx}(x, 0)/\sigma_0$ distributions for different values of the relative moving speed of the punch c under a frictional moving cylindrical punch, (a) $\mu_f = 0$, (b) $\mu_f = 0.25$ and (c) $\mu_f = 0.5$.

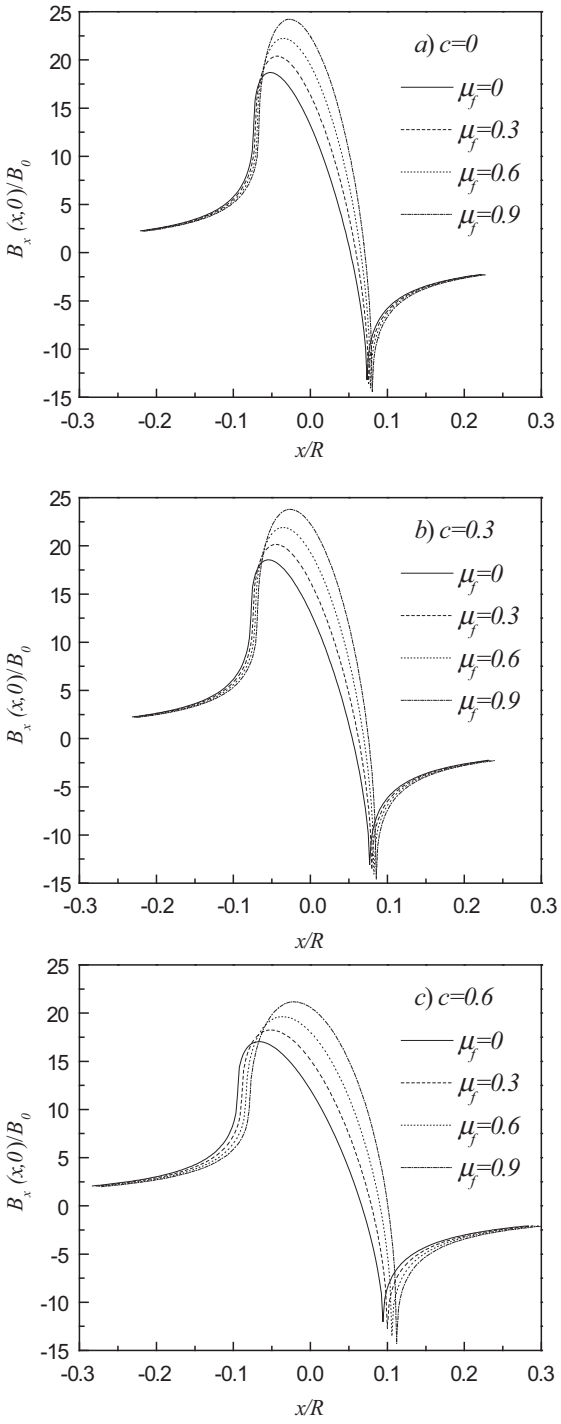

Fig. 13. The surface magnetic induction $B_x(x, 0)/B_0$ distributions for different values of the friction coefficient μ_f under a frictional moving cylindrical punch, (a) $c = 0$, (b) $c = 0.3$ and (c) $c = 0.6$.

either the friction coefficient or the moving speed of the punch becoming larger. The spike of the surface in-plane stress may cause the surface damage.

In addition, Figs. 11 and 12(a) show that the surface in-plane stress is symmetric and keeps free outside the contact region when $\mu_f = 0$, which is the same as the classic result on smooth contact for purely elastic materials.

Figs. 13 and 14 demonstrate the distributions of the surface magnetic induction $B_x(x, 0)/B_0$ ($B_0 = d_{33}P/(c_{33}R)$) under a frictional moving cylindrical punch for different values of the friction coefficient μ_f and the relative moving speed of the punch c. Unlike the surface in-plane stress, the surface magnetic induction has a negative spike at the edge $x = b$ of the cylindrical punch. The spike magnitude increases as the friction coefficient increases, while decreases as the cylindrical punch moves faster. The spike of the magnetic induction makes Terfenol-D vulnerable when subjected to the contact loading on the surface.

Like the frictional flat punch case, there may also exist a critical value c_0 for relative moving speed of the punch c in dynamic contact problem under a frictional cylindrical punch. Here $c_0 \approx 0.25$ as can be seen form Figs. 10, 12 and 14. When c varies between 0 and 0.25, the surface normal stress, surface in-plane stress and surface

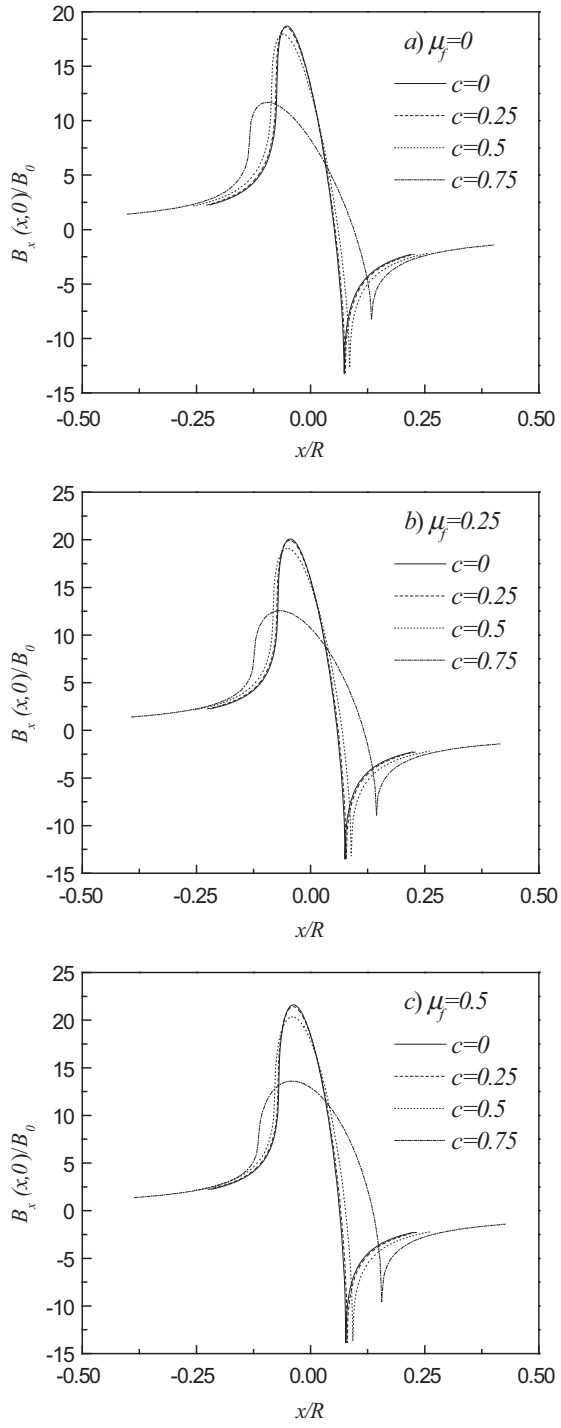

Fig. 14. The surface magnetic induction $B_x(x, 0)/B_0$ distributions for different values of the relative moving speed of the punch c under a frictional moving cylindrical punch, (a) $\mu_f = 0$, (b) $\mu_f = 0.25$ and (c) $\mu_f = 0.5$.

magnetic induction do not change much; while $c_0 > 0.25$, especially coming to 0.75, they change a lot.

5. Conclusions

Frictional moving contact model for piezomagnetic materials under a rigid punch is established. The rigid punch, possessing a flat or a cylindrical profile, moves at a constant speed. An important magnetostrictive material, Terfenol-D, is chosen for the derivation and numerical computation. Usage of the Galilean transformation and Fourier transform reduces the stated problem to Cauchy integral equations of the second kind. Exact solution is presented and explicit expressions of the physical quantities, including the contact stress, in-plane stress and magnetic induction on the surface are given in terms of elementary functions. Numerical experiments are implemented to reveal the influences of the friction coefficient and the moving velocity on the contact behavior. Following observations are made:

(i) Under a frictional moving flat punch, the surface magnetic induction magnitude is unbounded and discontinuous at both edges of the flat punch, which may explain why surface damage occurs for piezomagnetic materials besides the surface normal stress and surface in-plane stress.
(ii) The surface magnetic induction has a negative spike at the edge $x = b$ of the cylindrical punch, which, besides the stress components, may explain why surface damage occurs for piezomagnetic materials when subjected to a cylindrical punch.
(iii) Both the friction coefficient and the moving velocity affect the contact behaviors in its own way in the present frictional moving contact model.

These interesting observations may provide useful guidelines to the development of the indentation technique for piezomagnetic materials.

In the present model, the simple Coulomb friction law is utilized to obtain analytical solutions. The factor c (the relative moving speed of the punch) can be considered in the friction model where the velocity is important, such as the Stribeck friction model and the Karnopp model. The analytical solutions for moving contact problem involving piezomagnetic materials in case of the Stribeck friction model and the Karnopp model, which seem difficult, deserve to be treated in the forthcoming work.

Appendix A

1. The matrices $a_{mn}(m, n = 1, 2, 3)$ appearing in Eq. (29)

$$\begin{aligned}
a_{11} &= -i\cdot sign(\omega)[c_{13} \\
&\quad +c_{33}\tau_1 H_1(\tau_1) + d_{33}\tau_1 H_2(\tau_1)], \\
a_{12} &= -i\cdot sign(\omega)\{c_{13} + c_{33}[\mu_1\cdot \mathrm{Re}(H_1(\tau_2)) \\
&\quad -\nu_1\cdot \mathrm{Im}(H_1(\tau_2))] + d_{33}[\mu_1\cdot \mathrm{Re}(H_2(\tau_2)) - \nu_1\cdot \mathrm{Im}(H_2(\tau_2))]\}, \\
a_{13} &= -i\cdot sign(\omega)\{c_{33}[\mu_1\cdot \mathrm{Im}(H_1(\tau_2)) \\
&\quad +\nu_1\cdot \mathrm{Re}(H_1(\tau_2))] + d_{33}[\mu_1\cdot \mathrm{Im}(H_2(\tau_2)) + \nu_1\cdot \mathrm{Re}(H_2(\tau_2))]\}.
\end{aligned}$$

$$\begin{aligned}
a_{21} &= c_{44}[\tau_1 - H_1(\tau_1)] - d_{15}H_2(\tau_1), \\
a_{22} &= c_{44}[\mu_1 - \mathrm{Re}(H_1(\tau_2))] - d_{15}\mathrm{Re}(H_2(\tau_2)), \\
a_{23} &= c_{44}[\nu_1 - \mathrm{Im}(H_1(\tau_2))] - d_{15}\mathrm{Im}(H_2(\tau_2)).
\end{aligned} \tag{A.2}$$

$$\begin{aligned}
a_{31} &= -i\cdot sign(\omega)[d_{31} + d_{33}\tau_1 H_1(\tau_1) - \mu_{33}\tau_1 H_2(\tau_1)], \\
a_{32} &= -i\cdot sign(\omega)\{d_{31} + d_{33}[\mu_1\cdot \mathrm{Re}(H_1(\tau_2)) \\
&\quad -\nu_1\cdot \mathrm{Im}(H_1(\tau_2))] - \mu_{33}[\mu_1\cdot \mathrm{Re}(H_2(\tau_2)) - \nu_1\cdot \mathrm{Im}(H_2(\tau_2))]\}, \\
a_{33} &= -i\cdot sign(\omega)\{d_{33}[\mu_1\cdot \mathrm{Im}(H_1(\tau_2)) \\
&\quad +\nu_1\cdot \mathrm{Re}(H_1(\tau_2))] - \mu_{33}[\mu_1\cdot \mathrm{Im}(H_2(\tau_2)) + \nu_1\cdot \mathrm{Re}(H_2(\tau_2))]\}.
\end{aligned} \tag{A.3}$$

2. Expressions of $T_{kn}(k = 1, 2, n = 1, 2, 3)$ appearing in Eq. (37)

$$\begin{aligned}
T_{11} &= -i\cdot sign(\omega)[c_{11} + c_{13}\tau_1 H_1(\tau_1) + d_{31}\tau_1 H_2(\tau_1)], \\
T_{12} &= -i\cdot sign(\omega)\{c_{11} + c_{13}[\mu_1\cdot \mathrm{Re}(H_1(\tau_2)) \\
&\quad -\nu_1\cdot \mathrm{Im}(H_1(\tau_2))] + d_{31}[\mu_1\cdot \mathrm{Re}(H_2(\tau_2)) - \nu_1\cdot \mathrm{Im}(H_2(\tau_2))]\}, \\
T_{13} &= -i\cdot sign(\omega)\{c_{13}[\mu_1\cdot \mathrm{Im}(H_1(\tau_2)) + \nu_1\cdot \mathrm{Re}(H_1(\tau_2))] \\
&\quad +d_{31}[\mu_1\cdot \mathrm{Im}(H_2(\tau_2)) + \nu_1\cdot \mathrm{Re}(H_2(\tau_2))]\}.
\end{aligned} \tag{A.4}$$

$$\begin{aligned} T_{21} &= d_{15}[\tau_1 - H_1(\tau_1)] + \mu_{11} H_2(\tau_1), \\ T_{22} &= d_{15}[\mu_1 - \mathrm{Re}(H_1(\tau_2))] + \mu_{11}\mathrm{Re}(H_2(\tau_2)), \\ T_{23} &= d_{15}[\nu_1 - \mathrm{Im}(H_1(\tau_2))] + \mu_{11}\mathrm{Im}(H_2(\tau_2)). \end{aligned} \tag{A.5}$$

References

Affane, W., Gibbs, M.R.T., Powell, A.L., 1996. Performance modelling of micromachined sensor membranes coated with piezomagnetic material. Sens. Actuators A: Phys. 51, 219–224.

Chen, Q.N., Ma, F., Xie, S., Liu, Y., Proksch, R., Li, J., 2013. High sensitivity piezomagnetic force microscopy for quantitative probing of magnetic materials at the nanoscale. Nanoscale 5, 5747–5751.

Chen, T.Y., Nan, C.E., Weng, G.J., Chen, G.X., 2003. Unified approach for the estimate of effective magnetostriction of composites and polycrystals with particulate and columnar microstructures. Phys. Rev. B 68, 224406.

Chen, Y., Snyder, J.E., Schwichtenberg, C.R., Denni, K.W., Falzgraf, D.K., McCallum, R.W., Jiles, D.C., 1999. Effect of the elastic modulus of the matrix on magnetostrictive strain in composites. Appl. Phys. Lett. 74, 1159.

Erdogan, F., 1978. Mixed boundary value problems in mechanics. In: Nemat-Nasser, S. (Ed.), Mechanics Today, vol. 4. Pergamon Press, New York, pp. 1–86.

Feng, X., Fang, D.N., Soh, A.K., Hwang, K.C., 2003. Predicting effective magnetostriction and moduli of magnetostrictive composites by using the double-inclusion method. Mech. Mater. 35, 623–631.

Giannakopoulos, A.E., Parmaklis, A.Z., 2007. The contact problem of a circular rigid punch on piezomagnetic materials. Int. J. Solids Struct. 44, 4593–4612.

Guler, M.A., Erdogan, F., 2004. Contact mechanics of graded coatings. Int. J. Solids Struct. 41, 3865–3889.

Guler, M.A., Erdogan, F., 2007. The frictional sliding contact problems of rigid semi-parabolic and cylindrical stamps on graded coatings. Int. J. Mech. Sci. 49, 161–182.

Guo, Z.J., Busbridge, S.C., et al., 2001. Effective magnetostriction and magnetomechanical coupling of Terfenol-D composites. Appl. Phys. Lett 78, 3490.

Herbst, J.F., Capehart, T.W., Pinkerton, F.E., 1997. Estimating the effective magnetostriction of a composite: a simple model. Appl. Phys. Lett. 70, 3041.

Karl, W.J., Powell, A.L., Watts, R., Gibbs, M.R.J., Whitehouse, C.R., 2000. A micromachined magnetostrictive pressure sensor using magneto-optical interrogation. Sens. Actuators A: Phys. 81, 137–141.

Levin, V.M., 1967. Thermal expansion coefficients of heterogeneous materials. Mekh. Tverdogo Tela. 2, 88–94.

Lukashev, P., Sabirianov, R.F., Belashchenko, K., 2008. Theory of the piezomagnetic effect in Mn-based antiperovskites. Phys. Rev. B 78, 184414.

Moffet, M.B., Clark, A.E., Wun-Fogle, M., Linberg, J., Teter, J.P., McLaughlin, E.A., 1991. Characterization of Terfenol-D for magnetostrictive transducers. J. Acoust. Soc. Am. 89, 1445–1448.

Pinkerton, F.E., Cpehart, T.W., Herbst, J.F., Brewer, E.G., Murphy, C.B., 1997. Magnetostrictive SmFe2/metal composites. Appl. Phys. Lett. 70, 2601.

Shim, I.B., Bae, S.Y., Oh, Y.J., Choi, S.Y., 1998. Magnetic inhomogeneity in colossal magnetoresistive $La_{0.67}Ca_{0.33}MnO_{3-\delta}$ perovskite ceramics. Solid State Ionics 108, 241–247.

Singh, B.M., Rokne, J., 2013. Propagation of SH waves in layered functionally gradient piezoelectric–piezomagnetic structures. Philos. Mag. 93, 1690–1700.

Wu, T.L., Huang, J.H., 2000. Closed-form solutions for the magnetoelectric coupling coefficients in fibrous composites with piezoelectric and piezomagnetic phases. Int. J. Solids Struct. 37, 2981–3009.

Zhou, Y.T., Lee, K.Y., 2012. Exact contact analysis of piezomagnetic materials indented by a rigid sliding punch. Trans. ASME J. Appl. Mech. 79, 041011.

Zhou, Y.T., Lee, K.Y., 2013. Exact solutions of the 2-D frictional sliding contact problem of electrically insulated triangular and cylindrical punches on piezoelectric materials. ZAMM-Z Angew. Math. Mech. 93, 217–232.